Environmental Pollution 401 (2026) 128324

Contents lists available at ScienceDirect

Environmental Pollution

journal homepage: www.elsevier.com/locate/envpol

Polycyclic aromatic hydrocarbons in snow along a longitudinal transect in Chile from the Central Andes to the Antarctic Peninsula: Distribution, potential sources and atmospheric transport

América Metzdorff [a,*], Claudio Bravo [b], Francisco Fernandoy [c], Pirjo Huovinen [d,e], Rodrigo Loyola-Sepúlveda [f,g], Marco Salamanca [f,g], Claudio Bravo-Linares [a]

[a] Instituto de Ciencias Químicas, Facultad de Ciencias, Universidad Austral de Chile, Valdivia, Chile
[b] Centro de Estudios Científicos (CECs), Valdivia, Chile
[c] Laboratorio de Análisis Isotópico, Facultad de Ingeniería, Universidad Andrés Bello, Viña del Mar, Chile
[d] Instituto de Ciencias Marinas y Limnológicas, Universidad Austral de Chile, Valdivia, Chile
[e] Research Centre on Dynamics of High Latitude Marine Ecosystems (IDEAL), Valdivia, Chile
[f] Departamento de Oceanografía, Facultad de Ciencias Naturales y Oceanográficas, Universidad de Concepción, Concepción, Chile
[g] Laboratorio de Oceanografía Química (LOQ), Universidad de Concepción, Concepción, Chile

ARTICLE INFO

Keywords:
PAHs
Snow
Long-range atmospheric transport
HYSPLIT
Antarctic peninsula

ABSTRACT

This study investigates the occurrence, composition and potential sources of polycyclic aromatic hydrocarbons (PAHs) in snow and firn along a longitudinal transect from the Central Andes of Chile to the Antarctic Peninsula. Nineteen PAHs were quantified in 42 samples collected across five zones spanning high-elevation Andean catchments, snow- and ice-capped volcanoes and coastal Antarctic sites. Total PAH concentrations (Σ_{19}PAHs) show a clear along-transect gradient, with the highest mean values in the central-Andes zones and markedly lower concentrations in the Chilean Lake District and the Antarctic Peninsula. In all zones, the PAH mixture was dominated by low-molecular-weight (LMW) compounds (2–3 rings), indicating the prevalence of more volatile species consistent with medium-to long-range atmospheric transport. Diagnostic ratios (LMW/HMW, Ant/(Ant + Phe), Fla/(Fla + Pyr) of particle PAHs suggest predominantly petrogenic signatures across most zones, although these indicators are interpreted cautiously given their known limitations in remote snow and firn. Multivariate analysis of standardized PAH profiles further reveals a primary gradient in contamination intensity driven by high-molecular-weight PAHs and a secondary gradient associated with more volatile compounds (2-MeN, Flu and Acy), in agreement with the diagnostic ratios. HYSPLIT back-trajectory and trajectory-frequency analyses suggest a systematic shift from mixed oceanic–continental air masses in the Central Andes to predominantly maritime advection in Patagonia and Antarctica, which is consistent with the spatial patterns observed in ΣPAHs, LMW/HMW ratios and diagnostic source fields, and supports their interpretation in terms of changing air-mass origin. Overall, the results highlight the dominant role of long-range transport of petrogenic PAHs to remote cryospheric environments of the Southern Hemisphere, modulated by region-specific combustion sources along the transect.

1. Introduction

The cryosphere comprises regions of the Earth's surface where water persists in solid form, including glaciers, ice sheets, polar ice caps, seasonal snow and frozen ground such as permafrost (Barry, 2011). These environments are generally distant from urban centres and have limited direct human disturbance, which makes them some of the most pristine yet ecologically sensitive ecosystems worldwide (Liu et al., 2023; Qin et al., 2017). Within this system, the Andes mountain range constitutes an extensive high-elevation cryospheric region in South America, hosting a large diversity of glaciers from arid high-altitude ice bodies in the north to temperate ice fields in the humid south and containing the largest concentration of glacial ice in the Southern Hemisphere outside Antarctica (Davies et al., 2023). Antarctica represents the major

* Corresponding author. Instituto de Ciencias Químicas, Universidad Austral de Chile, Valdivia, Chile.
E-mail address: america.metzdorff@uach.cl (A. Metzdorff).

https://doi.org/10.1016/j.envpol.2026.128324
Received 28 January 2026; Received in revised form 8 May 2026; Accepted 10 May 2026
Available online 12 May 2026
0269-7491/© 2026 Published by Elsevier Ltd.

component of the global cryosphere, with almost its entire surface blanketed by ice and snow and a smaller area of exposed rock and unconsolidated deposits that record a complex geological, geomorphological and glaciological history (Cox et al., 2023; González et al., 2020). Against this background, snow and firn along the Andean–Antarctic transect provide an opportunity to use polycyclic aromatic hydrocarbons (PAHs) as tracers of atmospheric deposition and long-range transport, linking cryospheric archives to emission patterns and air-mass history (Strugnell et al., 2022).

High-latitude and high-altitude cryospheric regions function as environmental archives that capture and preserve contaminant deposition over time (Abakumov et al., 2021; Tin et al., 2009). Although often considered pristine, they are increasingly influenced by long-range transport of pollutants and by ongoing global environmental change (Abakumov et al., 2021; Cordero et al., 2022; Pawlak et al., 2021). Cryospheric bodies act as "cold condensers", efficiently scavenging atmospheric contaminants, with glaciers being able to retain pollutants for centuries and undergoing post-depositional processes such as re-volatilisation and vertical migration into deeper layers in response to thermal fluctuations and melt events, whereas fresh snow predominantly reflects more recent atmospheric deposition (Pawlak et al., 2021; Zhang et al., 2015). Numerous studies have documented anthropogenic contamination in cryospheric environments by pollutants such as sulphur (Pei et al., 2020), heavy metals (Chu et al., 2019; Puasa et al., 2021), Persistent Organic Pollutants (POPs) (Bhardwaj et al., 2018), and semi-volatile organic compounds (SVOCs). Owing to their low vapour pressure, SVOCs partition between the gas phase and condensed phases, becoming associated with airborne particles, settled dust and environmental surfaces (Cao et al., 2023; Wang et al., 2023; Wilson et al., 2021; Wu et al., 2022).

In this context, polycyclic aromatic hydrocarbons (PAHs) form a particularly informative class of SVOCs: they are composed of fused aromatic rings and are primarily generated during the incomplete combustion of organic matter (Wei et al., 2024; Wu et al., 2023a,b). Their phase partitioning, cold-condensation behaviour and efficient scavenging by snow and firn allow cryospheric archives to record both regional emission patterns and long-range transport signals, and PAHs have been widely detected in air, water, soil and biota across remote and urban regions (Bargagli and Rota, 2024; Bhardwaj et al., 2018).

The presence of PAHs in remote regions reflects a complex interplay between local and long-range atmospheric transport processes, with contributions from nearby human activities (e.g., research stations and tourism), distant industrial and urban emissions, maritime operations and, in some cases, natural sources such as volcanic eruptions (Wu et al., 2023a,b). Their accumulation in polar and high-altitude environments is favoured by low temperatures and reduced solar radiation, which increase their environmental residence times and persistence compared with lower-latitude regions (Kukučka et al., 2010).

Additional mechanisms contributing to the dispersion of pollutants in polar environments include long-range atmospheric transport (LRAT), oceanic currents and riverine pathways (Xie et al., 2022; Xie and Kallenborn, 2023). These processes play a key role in delivering contaminants to remote regions, where both local and distant sources can be relevant (Gebru et al., 2024; Wania and Mackay, 1995).

The aim of this study is to determine the presence, distribution and potential sources of PAHs along a longitudinal transect from the Central Andes to Antarctica, based on site-integrated snow and firn records. By analysing PAH concentrations in snow samples collected along Andean and Antarctic transects and interpreting them in conjunction with air-mass back-trajectory modelling, this study aims to resolve PAH levels, spatial patterns and source signatures in high-altitude and polar snow, thereby clarifying how long-range atmospheric transport contributes to PAH deposition in remote cryospheric environments.

2. Materials and methods

Snow samples were collected between 2015 and 2024 during several field campaigns conducted along a latitudinal transect extending from the Central Andes of Chile to the Antarctic Peninsula. In total, 42 samples were obtained from five zones (labelled A to E), including 36 surface snow samples and 6 firn core samples, to characterise the spatial variability of PAHs across cold environments of the Southern Hemisphere. The study zones were selected primarily based on logistical feasibility and site accessibility. Firn cores were homogenised and analysed as bulk samples to obtain sufficient volume for reliable PAH determination at trace levels and to ensure representative concentrations and were therefore used to characterise site-integrated PAH levels at each site rather than sub-annual temporal variability. Because samples within a given zone were not always collected in the same year, the dataset should be regarded as primarily spatial rather than temporal, and temporal variability can only be considered qualitatively in the present analysis.

Fig. 1 shows the sampling locations grouped into the five zones from north to south. Although 42 samples were analysed, fewer symbols are displayed on the map because several sites included replicate samples (e.g., A-LK-1, A-LK-2, A-LK-3) collected at the same point. Table SI1 summarises sampling design, including each zone, sample ID, sample type, sampling date and geographic coordinates and location.

2.1. Surface snow sampling

Most samples corresponded to surface snow (n = 36), representing recent atmospheric deposition. Surface snow was collected across all study zones – from high-elevation Andean catchments to polar environments following using pre-cleaned sampling tools and containers to minimise contamination. Sampling was conducted between January 2015 and September 2024 using a metal shovel to collect the upper 0–10 cm of snow. The material was transferred into 2 L glass jars and/or 2 L Whirl-Pak® bags (24 × 38 cm), with all containers pre-cleaned with acetone. Immediately after collection, samples were kept in the dark to prevent exposure to sunlight and stored at −20 °C until transport to the Laboratory at the Universidad Austral de Chile in the city of Valdivia (39°S).

2.2. Firn core sampling

Six firn core samples (n = 6) were retrieved from glacierised sites with suitable snow accumulation conditions at Juncal Sur (Central chilean Andes), Louis Philippe and O'Higgins glaciers (Antarctic Peninsula). Firn cores were collected between 2015 and 2022 using a 5.7 cm diameter electric drill (Icedrill.ch AG) following established protocols (Hoffmann-Abdi et al., 2023). Immediately after extraction, each core was measured, weighed and sealed in plastic bags, then stored in insulated containers to maintain low temperature. The cores were transported by helicopter and kept at −20 °C until arrival in Punta Arenas, Chile. From Punta Arenas, they were airlifted to Universidad Andrés Bello (Viña del Mar campus) and stored at −20 °C in a dedicated cold-storage facility until analysis (Fernandoy et al., 2018; Hoffmann-Abdi et al., 2023).

For PAH analysis, firn cores were homogenised and analysed as bulk samples to obtain sufficient volume for reliable GC–MS/MS determination at trace levels and to provide site-integrated PAH concentrations rather than high-resolution temporal profiles.

2.3. Sample processing and PAH extraction

The analytical workflow applied to all snow samples is summarised here. Upon arrival at the laboratory, samples were kept in the dark and allowed to melt at room temperature. The meltwater was then vacuum-filtered using a filtration unit equipped with pre-combusted glass fibre

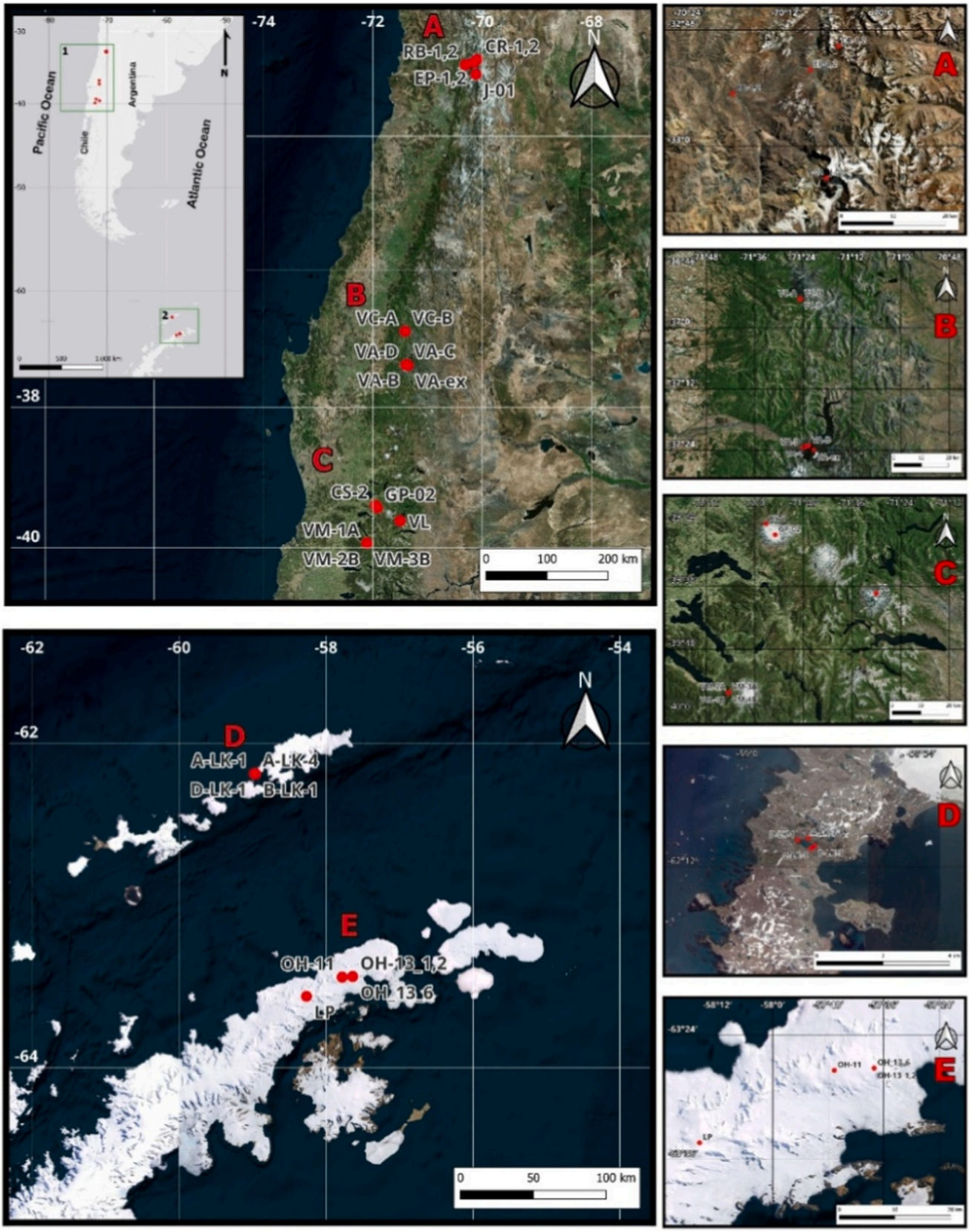


Fig. 1. Geographic location of the sampling transects from the Central Andes to the Antarctic Peninsula, including the sampling sites within each alphabetically designated zone (A to E). *Note that the figure shows sampling sites rather than the total number of samples, as some locations include replicated samples (*e.g., *A-LK-1, A-LK-2, A-LK-3).*

filters (e.g., GF/F), so that the particulate-associated PAH fraction was operationally retained on the filters, while the dissolved phase in the filtrate was not analysed. The volume of meltwater obtained from individual samples typically ranged between approximately 0.5 and 2 L. Concentrations are therefore reported in ng L^{-1}, normalised to the volume of melted snow, and represent particle-associated PAH burdens per unit volume of snow rather than total (particle + dissolved) PAH concentrations. The filters were subsequently extracted by microwave-assisted extraction (MAE), performing two extraction cycles with 20 mL of an acetone: n-hexane mixture (1:4, v/v), each run lasting 30 min. The combined extracts were concentrated to near dryness using a SuperVap evaporation system, transferred to pre-cleaned vials and reconstituted in 500 μL of isooctane. Final extracts were then prepared for analysis by gas chromatography coupled to tandem mass spectrometry (GC–MS/MS).

2.4. Sample analyses

PAHs were analysed using a TRACE™ 1300 gas chromatograph coupled to a TSQ 9000 triple-quadrupole mass spectrometer (Thermo Scientific), equipped with a TriPlus RSH autosampler operating in splitless injection mode. Electron ionisation was performed at 70 eV. Chromatographic separation was achieved on a TraceGOLD™ TG-PAH capillary column (30 m × 0.25 mm i. d. × 0.10 μm film thickness), specifically optimised for PAH determination. The GC oven temperature programme was as follows: initial hold at 60 °C for 4 min, ramp to 300 °C at 10 °C min^{-1}, followed by a final hold at 300 °C for 2 min. Helium was used as the carrier gas at a constant flow of 1.8 mL min^{-1}. The injector temperature was set to 290 °C and the transfer line to 300 °C. Mass spectrometric detection was carried out in selected-ion monitoring (SIM) mode, acquiring characteristic fragment ions for each target PAH for quantification. The collision energies (CE), retention times (RT) and product mass for each compound are provided in Table SI2.

2.5. PAHs quantification and method validation

A total of 19 PAHs were quantified: Naphthalene (Nap), 2-Methylnaphthalen (2-MeN), Acenaphthylene (Acy), Acenaphthene (Ace), Fluorene (Flu), Phenanthrene (Phe), Anthracene (Ant), Fluoranthene (Fla), Pyrene (Pyr), Benzo[c]Fluorene (B[c]F), Benz[a]Anthracene (B[a]A), Chrysene (Chr), Benzo[b]Fluoranthene (B[b]F), Benzo[k]Fluroanthene (B[k]F), Benzo[j]Fluroanthene (B[j]F), Benzo[e]Pyrene (B[e]P), Benzo [a]Pyrene (B[a]P), Indeno[1,2,3-c,d]Pyrene (IcdP) and Benzo[g,h,i] Perylene (BghiP). These compounds were selected to largely overlap with the U.S. EPA priority PAHs while including additional alkylated and high-molecular-weight congeners frequently used in atmospheric and cryospheric studies. This combination spans a broad range of molecular weights and volatilities, which is advantageous for investigating long-range atmospheric transport, deposition processes and source signatures in remote snowpacks.

Quantification and compound identification were based on multipoint calibration curves prepared from certified PAH standard mixtures supplied by Wellington Laboratories™, including internal (L429-IS), surrogate (L429-SS), recovery (L429-RS) and alternate (L429-AS) calibration and quality-control standards. Surrogate standards (L429-SS) were added to all samples immediately before the clean-up step on the silica gel/sodium sulphate/glass fibre column, by spiking the extracts prior to column chromatography, to monitor method performance, and their recoveries typically fell within 51–109%, confirming that the method performance was suitable for trace-level PAH determination in snow and firn. Uncorrected concentrations are reported, and, within this range, the lower recoveries mainly affect the most volatile PAHs, for which the reported values should be regarded as conservative.

A total of 44 samples were processed, including 42 environmental snow and firn samples and 2 field blanks collected during one of the field campaigns. The field blanks consisted of pre-cleaned sampling containers that were exposed and handled in the field like real samples, then filled with ultrapure water and analysed using the same protocol as environmental samples. PAH levels in these field blanks were below the detection limits and much lower than in environmental samples, indicating negligible contamination from sampling and transport. No separate procedural laboratory blanks were prepared; instead, method performance and background levels were evaluated using field blanks, calibration and quality-control standards, and preliminary method-validation tests used to establish instrumental detection limits and calibration behaviour for each PAH. Multi-level calibration curves, constructed from certified PAH standard mixtures and compound-specific relative response factors (RRFs), were linear over the working range ($R^2 > 0.99$ for all compounds). Instrumental limits of detection were then converted to sample-based LODs (ng L^{-1}) by considering the injection volume, extraction volume and filtered snow volume used in the method, yielding LODs between 0.1 and 0.5 ng L^{-1} (Table SI3). Because blank levels were below the detection limits, no blank correction was applied, and the reported concentrations correspond to uncorrected values. For each sample, the mass of each PAH determined in the filter extract was normalised by the volume of melted snow filtered, yielding concentrations expressed per liter of melted snow (ng L^{-1}). Therefore, the reported concentrations represent particle-associated PAHs on a volumetric basis, rather than total (particulate + dissolved) PAH concentrations in snow.

2.6. Diagnostic ratios for PAH source interpretation

In this study, PAHs were classified as low molecular weight (LMW), including compounds with 2–3 aromatic rings, and high molecular weight (HMW), including compounds with 4 or more aromatic rings.

Diagnostic ratios were used to support the interpretation of potential PAH sources and combustion processes influencing deposition across the study region. Three widely applied ratio sets were selected based on data availability and their documented use in cold and remote environments: (i) LMW/HMW versus ΣPAHs, (ii) Phe/Ant versus Fla/Pyr, and (iii) Ant/(Ant + Phe) versus Fla/(Fla + Pyr), which are commonly employed to distinguish petrogenic from pyrogenic signatures (Bhardwaj et al., 2018; Chen et al., 2018a; Han et al., 2023). In addition, some diagnostic plots were displayed on log–log scales (e.g. LMW/HMW versus ΣPAHs in Fig. 3 and Phe/Ant versus Fla/Pyr in Fig. SI1) to accommodate the wide dynamic range of the data and to better discriminate patterns at low ratio values.

These ratios were chosen following recommendations from reviews that critically assess the performance and limitations of PAH diagnostic indicators in atmospheric and cryospheric settings (Keyte et al., 2013a; Tobiszewski and Namieśnik, 2012; Yunker et al., 2002). Ratios were calculated only when all compounds involved were above method detection limits to minimise bias. Interpretations were made cautiously, considering contemporary guidance on the effects of long-range transport and the differential stability of PAHs under cold conditions (Keyte et al., 2013a; Tobiszewski and Namieśnik, 2012; Yunker et al., 2002).

2.7. Atmospheric transporting modelling using HYSPLIT

Backward air-mass trajectories were generated with the Hybrid Single-Particle Lagrangian Integrated Trajectory (HYSPLIT) model developed by NOAA's Air Resources Laboratory (ARL) (Stein et al., 2015). Trajectories were computed for representative sites within each sampling zone using Global Data Assimilation System (GDAS) 1° × 1° meteorological fields, with arrival heights set at 500 m above ground level to characterise boundary-layer and lower-tropospheric transport towards the snow surface.

We used 72-h back trajectories with an arrival height of 500 m as a compromise between capturing the recent transport history and

maintaining acceptable trajectory reliability in the mid-latitude and high-latitude circulation regimes considered here, consistent with previous PAH deposition studies using HYSPLIT (Fang et al., 2018). Longer trajectories (e.g. 96 h) and multi-height trajectory ensembles were not implemented in this study to keep the analysis tractable and focused on providing a qualitative transport context for the observed PAH gradients, but they represent a valuable extension for future work.

For each zone, 72 h backward trajectories were calculated at 6 h intervals over the sampling period. Trajectories were used solely to assess air-mass origin and transport pathways and to evaluate the potential atmospheric transport of contaminants from lower-latitude source regions towards the study sites, in line with previous applications of trajectory analysis in polar environments (Dickhut et al., 2005; Gambaro et al., 2005; Kallenborn et al., 1998). Trajectory calculation and visualisation were carried out using the NOAA HYSPLIT web interface.

2.8. Statistical analyses

Principal component analysis (PCA) was applied as an exploratory tool to summarize multivariate patterns in PAH concentrations measured in snow samples, reducing the dimensionality of the dataset while retaining most of its variability; the full description and biplot are provided in the Supplementary Material (Fig. SI3), while the main text focuses on a concise description of the dominant gradients represented by the first two principal components. Prior to analysis, concentrations of the nineteen selected PAHs were standardized using Z-scores, so that all variables contributed on a comparable scale, effectively performing the PCA on the correlation matrix. Missing values (mainly associated with concentrations < LOD) were imputed using the mean of each compound to obtain a complete samples-by-compounds matrix suitable for multivariate analysis. The PCA was conducted in Python (version 3.11.6) using the scikit-learn library (PCA function from the sklearn decomposition module), and the results were visualized as biplots showing simultaneously the sample scores and the contributions (loadings) of each PAH to the principal components (see Fig. SI3).

3. Results and discussion

3.1. Overview of PAH concentrations along the transect

Along the longitudinal transect considered in this study, the distribution of PAH concentrations in snow and firn is summarised in Table 1. For each of the five sampling zones (A–E), the table reports the number of samples, as well as the mean, minimum, maximum and standard deviation of ΣPAHs, together with the contributions of low- (ΣLMW) and high-molecular-weight (ΣHMW) compounds, providing a first-order view of latitudinal concentration patterns and potential signatures of large-scale atmospheric transport (Abramova et al., 2016). These concentrations refer to PAHs associated with the particulate fraction retained on the filters; dissolved PAHs in the meltwater were not quantified. Consequently, the values reported here represent particulate-bound PAHs expressed in ng L^{-1} of meltwater and may underestimate the total (particulate + dissolved) PAH burden, particularly for the more water-soluble LMW compounds, although the relative spatial patterns discussed along the transect are not affected.

According to Table 1, mean Σ_{19}PAH concentrations show a clear gradient along the transect. Zone B exhibits the highest average levels (1642 ± 519 ng L^{-1}), followed by zone A (653 ± 180 ng L^{-1}), whereas zones C (295 ± 95 ng L^{-1}), D (213 ± 36 ng L^{-1}) and E (260 ± 50 ng L^{-1}) display much lower mean values. LMW PAHs clearly dominate over HMW species in all zones, supporting the idea of a substantial contribution from more volatile and readily transported compounds, particularly at the most remote sites. (Keyte et al., 2013b; Yunker et al., 2002).

Conversely, HMW PAHs were relatively more enriched in zones B and D, which may reflect a stronger influence of nearby emission sources and/or deposition conditions that favour the retention of less volatile, particle-bound compounds (Keyte et al., 2013a).

Table SI4 reports mean concentrations and standard deviations of individual PAHs in the different zones. Overall, the zonal profiles indicate that LMW PAHs (2–3 rings), mainly Nap, 2-MeN, Ace and Phe, dominate the mixture, whereas HMW PAHs (4–6 rings) contribute only about 5-33% of ∑PAHs across the zones. This pattern is consistent with a scenario controlled by medium-to long-range atmospheric transport, in which the more volatile and semi-volatile compounds are efficiently redistributed before deposition onto snow and firn, in agreement with observations from other remote snow environments such as Ekström Ice Shelf and Ny-Ålesund (Lammel, 2015; Vecchiato et al., 2018). The ocurrence of this signal across all zones (A–E) suggests that, despite the differences in absolute concentrations, the regional PAH burden is shaped by a broadly similar combination of sources and transport processes.

Zones A and B exhibit particularly high mean concentrations of Nap and 2-MeN, together with very large standard deviations, pointing to episodic deposition events superimposed on a lower regional background. This behaviour indicates enhanced exposure to air masses that have recently interacted with combustion sources (urban, industrial and/or traffic-related), so that, in addition to hemispheric-scale transport, regional or sub-hemispheric inputs substantially amplify the load of light PAHs (Deka et al., 2024; Wang et al., 2015; Wu et al., 2023a,b).

In contrast, zones C, D and E show a pronounced attenuation of mean concentrations for all compounds, yet they preserve the same hierarchical pattern Nap ≈2-MeN > Phe > (Fla, Pyr), which is typical of remote settings where atmospheric transport and degradation act as the main filters rather than local proximity to emissions (Vilanova et al., 2001). This behaviour is consistent with an influence of regional and continental anthropogenic sources, mainly linked to fossil-fuel combustion and other SVOC emissions in urban, industrial and traffic-impacted areas of central Chile, as documented for southern-hemisphere mountain and urban atmospheres (Shunthirasingham et al., 2011). Nevertheless, the large distances between these emission regions and the remote high-altitude and polar sites, together with the qualitative nature of the back-trajectory analysis, mean that this influence should be regarded as indicative rather than quantitatively constrained.

HMW PAHs (BaA, Chr, BbF, BkF, BaP, BghiP, among others) occur at low concentration, often close to the analytical detection limit, in line with their strong association with particulate matter and limited potential for long-range transport to high-latitude or high-altitude regions. However, several of these compounds (e.g., BeP and BghiP) display

Table 1
Descriptive statistics of ∑PAH concentrations and LMW/HMW fractions across zones A–E. All concentrations are expressed as nanograms per liter (ng L^{-1}) of melted snow.

Zones	*Mean Latitude (°S)*	*n*	Mean (ng L^{-1})	SD(ng L^{-1})	Min(ng L^{-1})	Max(ng L^{-1})	∑LMW(ng L^{-1})	∑ HMW(ng L^{-1})
A	32.94	5	653	180	0.69	1249	2548	715
B	37.18	7	1642	519	0.11	3461	10,286	1209
C	39.81	11	295	95	0.13	919	3068	174
D	62.19	15	213	36	0.13	254	2150	1045
E	63.48	4	260	50	0.16	277	975	64

slightly higher mean concentrations in zones B and D, which may reflect deposition conditions that favour the retention of particle-bound material or a stronger influence of regional sources at these intermediate sectors of the transect. This subtle enrichment of HMW PAHs in B and D suggests that spatial variations affect not only the magnitude of ΣPAHs but also the quality of the PAH mixture, an aspect that is further explored using the LMW/HMW ratio and diagnostic source ratios in the following section. The overall scarcity of HMW PAHs is consistent with studies showing that these compounds are predominantly removed by gravitational deposition near their sources and exhibit limited transport capacity towards polar and high-altitude environments (Kallenborn, 2006; Keyte et al., 2013a).

In contrast, LMW- PAHs are more volatile and semi-volatile and therefore more prone to long-range atmospheric transport, whereas high-molecular-weight PAHs are mainly associated with particles and tend to be removed closer to their sources (Birks et al., 2017; Keyte et al., 2013a). Moreover, many combustion processes emit a substantial proportion of low-molecular-weight PAHs (e.g. naphthalene and related 2–3-ring species), which, combined with their higher mobility, contributes to their predominance in remote snow and firn.

Fig. 2 illustrates the fractional contribution of LMW PAHs to Σ_{19}PAHs in each zone. LMW PAHs account for between 67 and 95% of Σ_{19}PAHs, with particularly high fractions in zones B, C and E (>89%), confirming that the overall PAH burden along the transect is dominated by 2–3-ring compounds. This behaviour is consistent with observations from remote mountain lakes and polar snowpacks, where LMW and medium-molecular-weight species typically dominate due to their higher volatility and long-range transport potential, whereas HMW PAHs contribute only minor fractions to the dissolved and particulate phases (Vecchiato et al., 2024; Vilanova et al., 2001).

Zone D stands out by exhibiting the largest relative contribution of ΣHMW, close to one third of Σ_{19}PAHs, indicating a comparatively more particle-bound and less volatile mixture at this intermediate sector of the transect. Such an enrichment of HMW PAHs is agreement with the limited long-range transport capacity and more efficient local or regional deposition reported for these compounds in remote and polar environments. This pattern supports the interpretation that, while long-range transport of LMW PAHs controls the regional background, local to regional sources and deposition processes modulate the HMW fraction, particularly in zone D.

3.2. Diagnostic ratios for PAH source interpretation

In Fig. 3, the log–log plot of LMW/HMW versus ΣPAHs is divided into three interpretative bands that summarize how the relative contribution of light and heavy PAHs evolves along the transect. The lower band (LMW/HMW <1; HMW-dominated) groups samples where high-molecular-weight PAHs exceed the light fraction and thus indicate predominantly pyrogenic inputs, in line with the diagnostic criterion summarised by Tobiszewski and Namieśnik (2012) who proposed LMW/HMW <1 for combustion sources and >1 for petrogenic influence. The upper band (LMW/HMW >3; LMW-dominated) captures situations where light and medium-weight PAHs clearly dominate over HMW species; such conditions are consistent with observations from Svalbard surface snow and Arctic air, where long-range transport from Eurasia leads to a prevalence of 2–3-ring and medium-weight PAHs over strictly local HMW emissions. Between these end-members, the intermediate band ($1 \leq$ LMW/HMW ≤ 3) represents a transition regime in which mixed petrogenic–pyrogenic signatures are expected, analogous to the gradients in ∑LMW/∑HMW observed between mine-proximal and marine reference sites in Arctic coastal systems affected by coal mining (Steenhuisen and Van Den Heuvel-Greve, 2021; Yu et al., 2019).

In Fig. 3, most of the snow samples fall within the LMW-dominated band (LMW/HMW >3), whereas only a small subset plots in the HMW-dominated region (LMW/HMW <1), with the remaining points occupying this intermediate transition zone. This pattern is consistent with the widely used diagnostic criterion whereby LMW/HMW <1 is taken to indicate predominantly pyrogenic inputs, while LMW/HMW >1 reflects petrogenic influence, as summarised by Tobiszewski and Namieśnik (2012) and subsequent applications in soils and sediments. The LMW-dominated samples include most sites from Zones C–E, which also encompass the highest ΣPAHs, suggesting that long-range transport of more volatile LMW PAHs and local perturbations linked to fuel handling or traffic near glacial and coastal settings are superimposed on regional background pollution, consistent with studies in Svalbard and other Arctic locations (Vecchiato et al., 2018). By contrast, the samples with LMW/HMW <1 occur mainly in Zone D at comparatively moderate ΣPAHs, pointing to episodes with a stronger pyrogenic signature that resemble the combustion-dominated end-members reported for urban and roadside snow in northern Russia and for roadside snowbanks used as passive samplers of traffic-related pollutants (Kozhevnikov et al., 2021; Müller et al., 2022). Similar separation between petrogenic and pyrogenic regimes using ∑LMW/∑HMW has been described in Arctic coastal systems affected by coal mining, where mine-proximal sites show elevated LMW/HMW relative to more remote marine locations, underscoring the sensitivity of this ratio to local point sources in otherwise remote regions (Steenhuisen and Van Den Heuvel-Greve, 2021).

The dominance of LMW-enriched samples in Fig. 3 therefore aligns with observations from Svalbard surface snow and Arctic air, where LMW and medium-weight PAHs transported from Eurasia outweigh strictly local HMW emissions, while the coexistence of a minority of HMW-dominated points highlights the episodic impact of combustion plumes along the Andean–Antarctic gradient (Drotikova et al., 2020; Vecchiato et al., 2024; Yu et al., 2019).

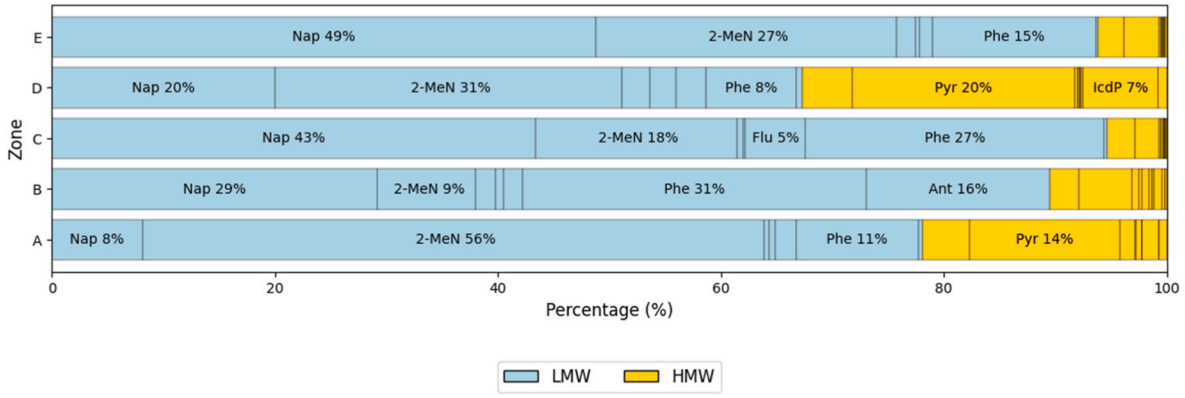


Fig. 2. PAH composition by Zone.

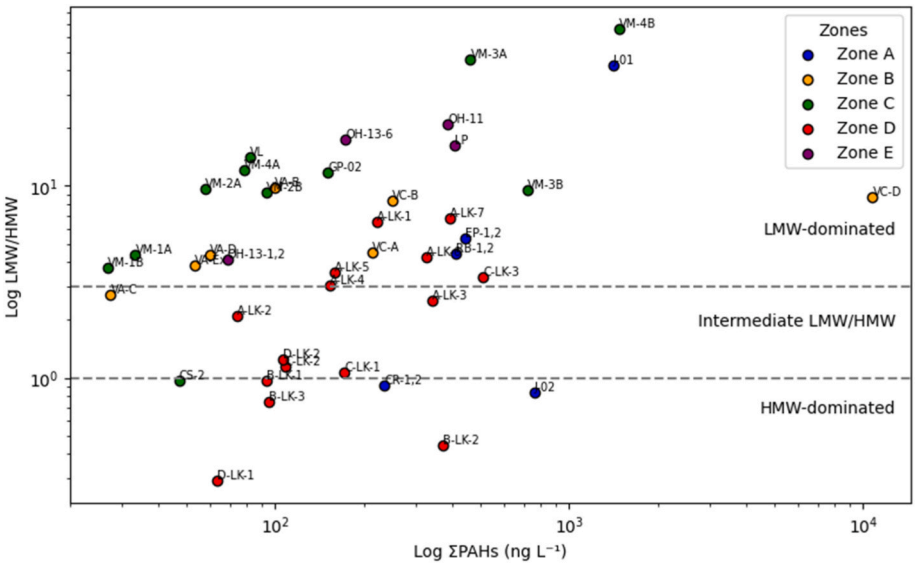


Fig. 3. The ΣPAHs versus Ratio LMW/HMW in Snow Along the different sample zones.

3.3. Diagnostic ratios Ant/(Ant + Phe) vs Fla/(Fla + Pyr) in snow samples

Diagnostic ratios based on selected pairs of PAHs are widely applied to infer potential sources and transformation pathways of these compounds in environmental matrices. In particular, the ratios Ant/(Ant + Phe) and Fla/(Fla + Pyr) have been extensively used to distinguish between petrogenic and pyrogenic origins, as well as to assess the relative contribution of combustion processes. Snow samples represent a unique medium for such analyses, as they act both as temporary reservoirs and as integrators of recent atmospheric deposition in cold regions. Although PAH diagnostic ratios in snow can provide insights into long-range transport patterns, the relative influence of local emission sources, and the apparent stability of these compounds under extreme climatic conditions, they may also be influenced by post-depositional processes (e.g. partial revolatilization, snowmelt and melt–freeze redistribution) and should therefore be interpreted as semi-quantitative indicators rather than perfectly conserved atmospheric fingerprints (Vecchiato et al., 2024). In addition, differential degradation and photochemical processing, particularly affecting the more labile LMW PAHs, can modify Ant/(Ant + Phe) and Fla/(Fla + Pyr) during long-range transport and residence in the snowpack, potentially driving ratios towards more intermediate values and partially obscuring the original source signatures. This section presents the diagnostic ratio analysis for the studied snow samples, highlighting source attribution patterns and their implications for contaminant dynamics in polar environments. In our dataset, the Ant/(Ant + Phe) (Yunker et al., 2002) and Fla/(Fla + Pyr) (Davis et al., 2019; Salat et al., 2021) ratios mostly fall within ranges typically associated with combustion-derived PAHs, indicating a predominantly pyrogenic influence rather than purely petrogenic inputs with higher-temperature fossil-fuel combustion signatures more common at the central Andean sites and more mixed or aged pyrogenic signatures towards the Antarctic locations.

For Ant/(Ant + Phe), diagnostic thresholds follow (Yunker et al., 2002) with values ≤ 0.10 indicating petrogenic inputs and values > 0.10 indicating pyrogenic (combustion) signatures. For Fla/(Fla + Pyr), ratios <0.40 were taken to indicate petrogenic sources, values between 0.40 and 0.50 liquid fossil fuel combustion, and values > 0.50 grass/-wood/coal combustion, following commonly applied PAH diagnostic thresholds (Davis et al., 2019; Salat et al., 2021).

However, these diagnostic ratios must be interpreted with caution in our long-range transport setting. Numerous studies, such as those by Katsoyiannis et al. (2007); Tobiszewski and Namieśnik (2012); Yunker et al. (2002) have shown that PAH diagnostic ratios can be altered during atmospheric transport and environmental degradation. In particular, Tobiszewski and Namieśnik (2012) reported that anthracene and phenanthrene do not degrade at the same rate in air, which can bias the Ant/(Ant + Phe) ratio as air masses age. Similar, although less pronounced, effects are likely for fluoranthene and pyrene, and thus for Fla/(Fla + Pyr), particularly under prolonged exposure to solar radiation during transport. In this study, we therefore apply these ratios as qualitative indicators only and interpret them together with the overall PAH composition and air-mass trajectories, rather than as precise quantitative source apportionment tools.

In Fig. 4, the diagnostic plot of Ant/(Ant + Phe) versus Fla/(Fla + Pyr) shows that most snow samples cluster within the petrogenic field defined by Ant/(Ant + Phe) < 0.10 and Fla/(Fla + Pyr) < 0.40, with a smaller number extending into the bands associated with liquid fossil-fuel combustion (0.40–0.50 in Fla/(Fla + Pyr)) and grass/wood/coal combustion (Fla/(Fla + Pyr) > 0.50). These thresholds follow the scheme originally proposed by Chen et al. (2018a,b); Davis et al. (2019); Neira et al. (2017) and Yunker et al. (2002) in another type of samples, whereby Ant/(Ant + Phe) < 0.10 and low Fla/(Fla + Pyr) values indicate petrogenic inputs, intermediate Fla/(Fla + Pyr) (0.40–0.50) reflects liquid fuel combustion, and high Fla/(Fla + Pyr) (>0.50) is typically associated to biomass and coal combustion; this framework has been widely adopted in subsequent studies of river water, sediments and atmospheric particles (Chen et al., 2018b; Yunker et al., 2002). Within the petrogenic band, samples from all zones are present, but Zones C and D contribute most of the sampling, suggesting that a regionally consistent petroleum-related background—potentially linked to long-range transport of volatilised petrogenic PAHs and diffuse fuel use along the transect—underlies the snow chemistry (Aslam et al., 2022).

The interaction of each zone with the combustion derived PAH profiles provides additional information on local versus regional sources. In Zone A, a subset of samples moves toward the liquid-fuel combustion band (Fla/(Fla + Pyr) $\approx$ 0.4–0.5 while Ant/(Ant + Phe) remains <0.1), consistent with emissions from vehicular traffic and other petroleum combustion sources, as reported for urban and roadside environments where these ratios shift from the purely petrogenic field into the mixed or liquid-fuel domain (Yunker et al., 2002; Zhang et al., 2015).

Zones B and C include isolated points in the grass/wood/coal combustion band (Fla/(Fla + Pyr) > 0.5, Ant/(Ant + Phe) > 0.10),

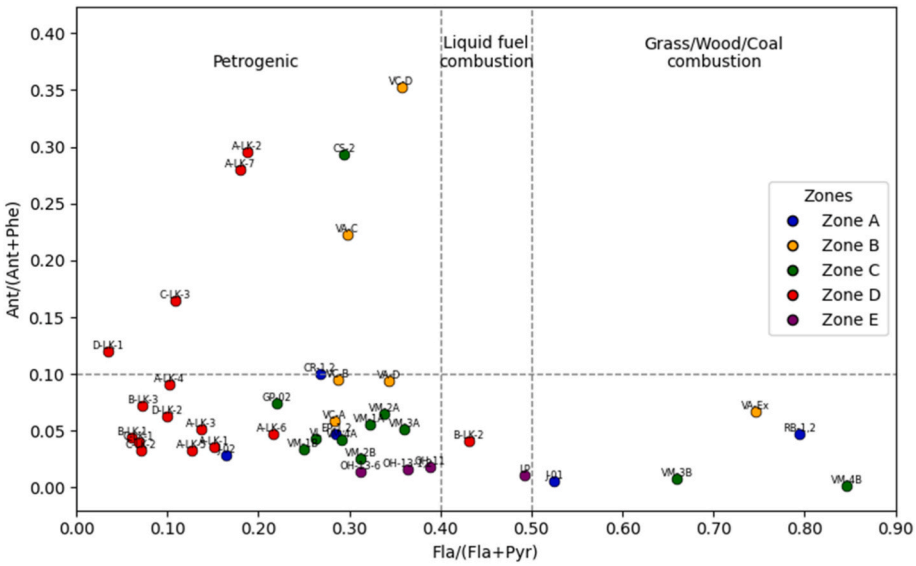


Fig. 4. Biplot of Ant/(Ant + Phe) versus Fla/(Fla + Pyr) for surface snow and firn samples from Zones A–E. The *horizontal dashed line at Ant/(Ant + Phe) = 0.10 separates petrogenic (≤0.10) from pyrogenic (combustion) signatures. Vertical dashed lines at Fla/(Fla + Pyr) = 0.40 and 0.50 distinguish petrogenic sources (<0.40), liquid fossil fuel combustion (0.40–0.50) and grass/wood/coal combustion (>0.50), following commonly applied PAH diagnostic thresholds.*

indicating episodic influence of biomass or coal burning superimposed on an otherwise petrogenic background, a behaviour similar to that described in high-latitude and coastal systems where residential heating or power generation episodes temporarily drive the ratios toward the combustion end-members. In contrast, Zone D spans the full range from clearly petrogenic to combustion-dominated signatures, with several samples plotting above Ant/(Ant + Phe) = 0.10 and into the grass/wood/coal field, pointing to a stronger and more variable pyrogenic imprint. This enhanced pyrogenic influence is consistent with the presence of local combustion sources on the Antarctic Peninsula, particularly vehicular traffic and aircraft operations around the Teniente Marsh airstrip on King George Island, superimposed on the regional long-range transport background. (see Fig. 4).

Finally, Zone E samples remain largely within or close to the petrogenic field but show modest excursions toward the liquid-fuel combustion band, suggesting relatively clean background air masses occasionally affected by local or regional fossil-fuel burning, as has been observed in other remote cryospheric settings where diagnostic ratios reveal subtle deviations from purely petrogenic signatures (Aslam et al., 2022; Davis et al., 2019).

3.3.1. *Zone-specific patterns in ant/(Ant+Phe)–Fla/(Fla+Pyr) ratios*

In Fig. 4, the diagnostic plot shows that most samples fall within the petrogenic band, with only a limited number of points entering the combustion fields, underscoring the overall dominance of petroleum-related signatures modulated by episodic combustion inputs. According to the widely used scheme of Yunker et al. (2002), Ant/(Ant + Phe) < 0.10 combined with Fla/(Fla + Pyr) < 0.40 indicates petrogenic sources, whereas Fla/(Fla + Pyr) between 0.40 and 0.50 is typical of liquid fossil-fuel combustion and Fla/(Fla + Pyr) > 0.50 with Ant/(Ant + Phe) > 0.10 reflects biomass and coal burning. In this framework, Zones A–E contribute 35 samples to the petrogenic field, 2 samples to the liquid-fuel combustion band (D:1, E:1) and 5 samples to the grass/wood/coal combustion band (A:2, B:1, C:2), highlighting that combustion signatures are present but remain secondary relative to the petrogenic background.

Zone A illustrates a mixed behaviour: three samples lie within the petrogenic domain, while two points fall in the biomass/coal combustion band, indicating that fuel-derived inputs coexist with episodic contributions from combustion of grass, wood or coal (Kozhevnikov et al., 2021). This pattern is consistent with studies in cryospheric and coastal environments where diagnostic ratios reveal predominantly petrogenic PAHs punctuated by events of domestic heating or other solid-fuel combustion that shift individual samples into the grass/wood/coal field (Iriarte et al., 2023).

Zone B is still dominated by petrogenic signatures (five samples in the blue band), but the presence of one point in the biomass/coal combustion region suggests a possible influence of more strongly pyrogenic plumes. Given that this indication is based solely on diagnostic ratios and that no independent evidence (e.g. information on regional fires, detailed back-trajectory analysis or additional tracers) is available, this potential contribution from biomass or coal combustion should be regarded as tentative.

Zone C shows the largest number of petrogenic samples (nine in the blue band) together with two points in the biomass/coal combustion band, supporting the view that this part of the transect is mainly controlled by petroleum-related PAHs with superimposed episodes of solid-fuel combustion. Zone D is the most complex: fourteen samples fall within the petrogenic range, but one point enters the liquid-fuel combustion band, indicating that, in addition to the regional petrogenic background, there are localised inputs from combustion of liquid fossil fuels, as commonly seen in areas influenced by traffic or fuel handling (Thompson et al., 2022; Tobiszewski and Namieśnik, 2012).

Finally, Zone E contributes three petrogenic samples and one in the liquid-fuel band, consistent with a relatively clean background where petroleum-derived PAHs dominate but intermittent fossil-fuel combustion episodes can still be detected in the diagnostic ratios.

An additional diagnostic plot using the alternative ratios Phe/Ant versus Fla/Pyr is provided in the Supporting Material (Figure SI1) and this log–log representation confirms the zone-specific patterns identified in the Ant/(Ant + Phe)–Fla/(Fla + Pyr) space, with samples from Zones A–E occupying consistent regions of the diagram and only a few points deviating toward more combustion-like signatures in line with previous applications of these ratios in aquatic and atmospheric environments.

In this section, we rely primarily on two families of diagnostic ratios: the bulk LMW/HMW index, which reflects the balance between more volatile, low-molecular-weight PAHs and less volatile high-molecular-weight species, and the paired Ant/(Ant + Phe) and Fla/(Fla + Pyr) ratios, which are commonly used to distinguish between petrogenic and combustion-related sources. While these ratios provide useful first-order constraints on PAH mixture characteristics, their interpretation is subject to important uncertainties, particularly under cold and remote

conditions. Differential degradation, phase partitioning and photochemical processing can affect individual compounds within each pair or group to different extents, potentially shifting the LMW/HMW balance and moving Ant/(Ant + Phe) and Fla/(Fla + Pyr) values away from their original source signatures (Tobiszewski and Namieśnik, 2012; Yunker et al., 2002).

These effects are likely to be enhanced during medium-to long-range atmospheric transport, where LMW compounds can be preferentially transported and HMW species more efficiently removed, and where photochemical aging may alter the relative abundance of anthracene versus phenanthrene and fluoranthene versus pyrene. As a result, the diagnostic fields classically defined for Ant/(Ant + Phe) and Fla/(Fla + Pyr) should be regarded as qualitative reference domains rather than strict, immutable thresholds, especially in polar and high-altitude environments (e.g. Yunker et al., 2002; diagnostic-ratio reviews). In our transect, we therefore use LMW/HMW and Ant/(Ant + Phe)–Fla/(Fla + Pyr) ratios as qualitative indicators to be interpreted jointly with concentration gradients, mixture composition and air-mass back--trajectories, and we explicitly acknowledge that they cannot on their own provide definitive, quantitative source apportionment.

3.4. Atmospheric transport patterns using HYSPLIT-NOAA

Backward-trajectory and trajectory-frequency analyses were used to link the observed gradients in PAH concentrations and diagnostic ratios to large-scale and regional air-mass transport along the transect. HYSPLIT 72-h back trajectories and associated frequency maps were calculated for each sampling day and site, following standard procedures widely applied in source–receptor studies of PAHs and other semi-volatile pollutants (Kubo et al., 2020; Miura et al., 2019; Szopińska et al., 2019). These tools have been extensively used to distinguish between oceanic and continental air masses and to identify periods when advection from specific source regions (e.g. East Asia, Europe, South America) enhances PAH levels at remote sites (Draxler and Hess, 2014).

Fig. 5 shows the HYSPLIT trajectory-frequency maps, revealing a coherent evolution of air-mass origin along the Central Andes–Antarctic transect. From the Central Chilean Andes (Zones A–C) to the Patagonian and Antarctic sites (Zones D–E), the circulation progressively shifts from mixed oceanic–continental flows, with an increasing influence of coastal and urban corridors, to predominantly maritime advection in the Antarctic sector. This large-scale transition provides a physical framework to interpret the along-transect gradients in ΣPAHs, LMW/HMW ratios and diagnostic fields, as detailed below for each zone (see Fig. 5). Additional information on the synoptic-scale transport patterns is provided in the Supporting Material, where Figure SI2 reports, for each zone, the 72-h backward-trajectory clusters derived from the HYSPLIT simulations, illustrating the typical pathways of air masses reaching the sampling sites and complementing the trajectory-frequency maps.

For Zone A, trajectory frequencies show that air masses during the sampling period travelled predominantly over the southeastern Pacific Ocean, with only a short final segment over central Chile before reaching the Andean site. This pattern is consistent with the predominance of petrogenic signatures and LMW-dominated PAHs in Zone A, with only a few samples shifting into the liquid-fuel and grass/wood/coal combustion fields in the Ant/(Ant + Phe)–Fla/(Fla + Pyr) diagram, indicating that a regional oceanic background is only weakly modulated

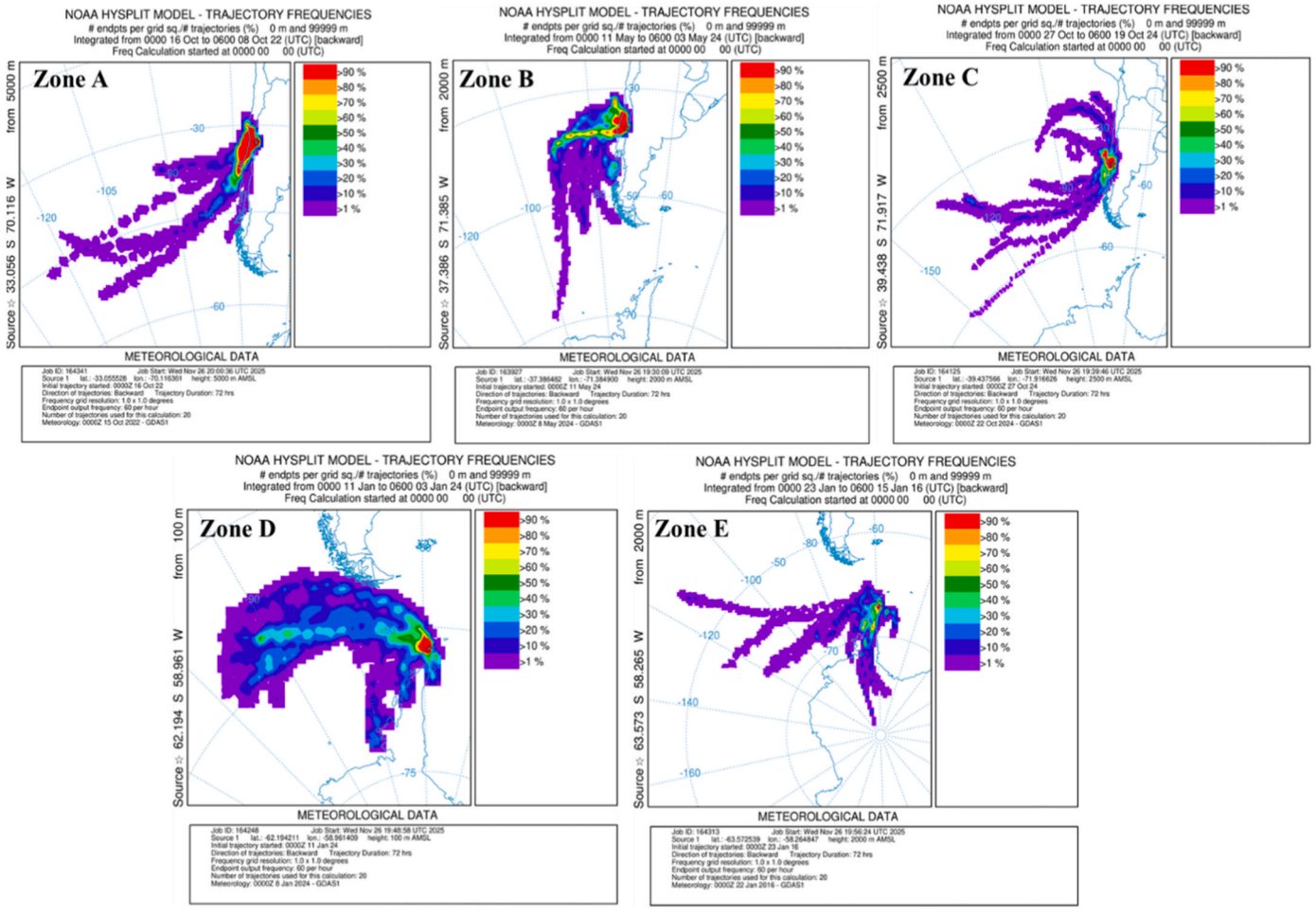


Fig. 5. Frequency of occurrence of trajectories calculated with the HYSPLIT model over the different study zones during the sampling period.

by combustion sources along the final continental pathway. In Zone B, air masses still originate mainly over the Pacific, but the highest trajectory frequencies are aligned with the coastal and central-southern corridor of Chile, implying longer residence times over urban and industrial areas. This agrees with the higher ΣPAHs, the presence of a few samples in the biomass/coal combustion band, and the stronger variability in diagnostic ratios relative to Zone A (see Figs. 3 and 4) similar to patterns reported in studies where trajectories crossing populated regions show enhanced pyrogenic fractions (Miura et al., 2019).

The Zone C displays a more complex frequency pattern, with a concentrated core over the central–southern coast and several branches extending over the southeastern Pacific, indicating alternating influence of oceanic and coastal air masses as another study reported by Vecchiato et al. (2024). This configuration explains why Zone C contains the largest number of petrogenic samples while still exhibiting several points in the biomass/coal combustion band and elevated ΣPAHs, reflecting a petroleum-dominated background periodically overprinted by solid-fuel combustion from southern Chile.

In contrast, Zones D and E, located in the Antarctic sector, are characterized by trajectories and peaks in trajectory frequency almost entirely confined to the ocean around the Antarctic Peninsula and the Scotia Sea, with very limited interaction with densely populated continental regions (Hayakawa et al., 2019; Szopińska et al., 2019). This predominance of maritime advection is consistent with their moderate ΣPAHs and overwhelmingly petrogenic signatures, with only a few samples drifting toward the liquid-fuel combustion band, as also observed in Antarctic and sub-Arctic studies where long-range transport from mid-latitudes delivers mainly LMW and medium-weight PAHs and only a weak imprint from local combustion activities (Drotikova et al., 2020; Hegg et al., 2010; Ma et al., 2013).

It is important to note that Zone D samples were collected during austral summer 2024, whereas Zone E samples correspond to austral summers 2015–2016; thus, part of the difference in their HYSPLIT trajectory-frequency patterns reflects interannual variability in large-scale circulation rather than purely spatial contrasts along the transect (Stein et al., 2015).

Overall, the HYSPLIT analysis is used here as a qualitative tool to characterise dominant air-mass pathways and to provide physical context for the observed PAH gradients, rather than as a fully quantitative source–receptor model. A more comprehensive assessment combining longer and multi-height back trajectories with fire and emission inventories and boundary-layer diagnostics (e.g. MODIS and GFED fire products) would be a valuable avenue for future, more modelling-intensive studies.

3.5. Global PCA biplot of PAHs

A global principal component analysis (PCA) was performed on the standardized concentrations of 20 PAHs measured in all snow samples to explore multivariate patterns in the dataset. The first principal component predominantly reflects the overall ΣPAH gradient and separates a small number of higher-load samples from the bulk of relatively low-load samples, whereas the second component explains a comparatively small fraction of the variance and does not reveal additional interpretable structure. Overall, the PCA simply confirms that the dominant feature of the dataset is a contamination-intensity gradient, consistent with the concentration patterns and diagnostic ratios discussed above and is therefore used only as supporting exploratory information; the complete biplot is provided in the Supplementary Material (Fig. SI3).

4. Conclusions

Across the Central Andes (Zone A), South-Central Chile (Zone B), Chilean Lake District (Zone C) and Antarctic Peninsula transect (Zone D and E), snow and firn exhibit a north-south decreasing ΣPAH concentrations and a mixture strongly dominated by low-molecular-weight compounds, indicating that the regional PAH burden is primarily controlled by more volatile species capable of medium-to long-range atmospheric transport. This behaviour is consistent with the longer atmospheric residence times and greater transport potential of LMW-PAHs reported by global-scale modelling and review studies (Friedman and Selin, 2012). Diagnostic ratios LMW/HMW, Ant/(Ant + Phe) and Fla/(Fla + Pyr) place most samples within the petrogenic field, with liquid-fuel and grass/wood/coal combustion signatures restricted to a minority of cases, suggesting a large-scale petroleum-related background episodically overprinted by regional combustion inputs that vary among zones. Similar LMW-dominated and petrogenic-type PAH mixtures have been reported in Antarctic snow and coastal environments influenced by station activities and marine transport (Na et al., 2011).

In the Antarctic Peninsula, this petrogenic-type background is consistent with the combined influence of petroleum-derived fuels used at research stations, marine transportation emissions and other local anthropogenic activities, superimposed on long-range transported PAHs (Iriarte et al., 2023; Na et al., 2011; Van Overmeiren et al., 2024).

The global PCA integrates these findings in a first component that represents a contamination-intensity gradient: PC1 separates the highly contaminated sample from the rest and shows stronger positive loadings for high-molecular-weight PAHs (including Fla and other 4–6-ring compounds), in agreement with the higher Σ~19~PAHs and combustion-type Ant/(Ant + Phe) and Fla/(Fla + Pyr) ratios found at those sites. In contrast, PC2 is largely driven by specific low-molecular-weight and alkylated PAHs (notably 2-MeN, Flu and Acy), capturing secondary variability in the more volatile, petrogenic-leaning fraction of the mixture and reflecting changes in volatility-driven transport and deposition rather than a distinct combustion source category.

Along the transect, the observed north–south gradients in ΣPAHs and diagnostic ratios are consistent with a systematic shift in air-mass origin from mixed oceanic–continental influences over the Central Andes to predominantly maritime advection in Patagonian and Antarctic sectors, as suggested by the HYSPLIT back-trajectory analysis. These HYSPLIT trajectories provide qualitative information on likely transport pathways and air-mass history, rather than quantitative source apportionment or deposition efficiencies, and are therefore used here as a physical framework to interpret the observed spatial patterns rather than to derive explicit source contributions. In this sense, our conclusions about source types and long-range transport are intended as qualitative, first-order inferences consistent with reported atmospheric residence times and PAH transport to remote and polar regions, rather than as the result of a full quantitative source-apportionment analysis (Friedman and Selin, 2012; Iriarte et al., 2023; Na et al., 2011; Van Overmeiren et al., 2024).

CRediT authorship contribution statement

América Metzdorff: Writing – review & editing, Writing – original draft, Visualization, Validation, Software, Resources, Project administration, Methodology, Investigation, Funding acquisition, Formal analysis, Data curation, Conceptualization. **Claudio Bravo:** Writing – review & editing, Investigation. **Francisco Fernandoy:** Writing – review & editing, Resources, Investigation. **Pirjo Huovinen:** Writing – review & editing, Resources, Investigation. **Rodrigo Loyola-Sepúlveda:** Supervision, Methodology, Formal analysis. **Marco Salamanca:** Supervision. **Claudio Bravo-Linares:** Writing – review & editing, Supervision, Methodology, Funding acquisition.

Ethics approval and consent to participate

The research in the Antarctic was carried out under the permission granted by Instituto Antártico Chileno (INACH) in accordance with the Protocol on Environmental Protection to the Antarctic Treaty.

Funding sources

This work was supported by ANID FONDECYT Postdoctoral 2023 N°3230504, ANID FONDECYT N°1201053, N°1242028, N° 1241670 and FONDAP N°15150003.

Declaration of competing interest

The authors declare that they have no known competing financial interests or personal relationships that could have appeared to influence the work reported in this paper.

Acknowledgements

We are grateful to T. Vicuña and D. Osman for their invaluable help in the field work in the Fildes Peninsula. The logistical support provided by the Instituto Antártico Chileno (INACh) and the staff at the Base Julio Escudero Station is also greatly acknowledged.

Appendix A. Supplementary data

Supplementary data to this article can be found online at https://doi.org/10.1016/j.envpol.2026.128324.

Data availability

Data will be made available on request.

References

Abakumov, E., Nizamutdinov, T., Yaneva, R., Zhiyanski, M., 2021. Polycyclic aromatic hydrocarbons and potentially toxic elements in soils of the vicinity of the Bulgarian antarctic station "St. Kliment Ohridski" (antarctic peninsula). Front. Environ. Sci. 9, 656271. https://doi.org/10.3389/fenvs.2021.656271.

Abramova, A., Chernianskii, S., Marchenko, N., Terskaya, E., 2016. Distribution of polycyclic aromatic hydrocarbons in snow particulates around longyearbyen and barentsburg settlements. Spitsbergen. Polar Rec. 52, 645–659. https://doi.org/10.1017/S0032247416000243.

Aslam, R., Sharif, F., Baqar, M., Shahzad, L., 2022. Source identification and risk assessment of polycyclic aromatic hydrocarbons (PAHs) in air and dust samples of lahore city. Sci. Rep. 12, 2459. https://doi.org/10.1038/s41598-022-06437-8.

Bargagli, R., Rota, E., 2024. Environmental contamination and climate change in antarctic ecosystems: an updated overview. Environ. Sci. Adv. 3, 543–560. https://doi.org/10.1039/D3VA00113J.

Barry, R.G., 2011. The cryosphere – past, present, and future: a review of the frozen water resources of the world. Polar Geogr. 34, 219–227. https://doi.org/10.1080/1088937X.2011.638146.

Bhardwaj, L., Chauhan, A., Ranjan, A., Jindal, T., 2018. Persistent organic pollutants in biotic and abiotic components of antarctic pristine environment. Earth Syst. Environ. 2, 35–54. https://doi.org/10.1007/s41748-017-0032-8.

Birks, S.J., Cho, S., Taylor, E., Yi, Y., Gibson, J.J., 2017. Characterizing the PAHs in surface waters and snow in the athabasca region: implications for identifying hydrological pathways of atmospheric deposition. Sci. Total Environ. 603–604, 570–583. https://doi.org/10.1016/j.scitotenv.2017.06.051.

Cao, J., Zhu, Y., Huang, X., Zhang, L., Wang, X., Geng, C., Huang, H., 2023. Role of dust loading in dynamic transport of semi-volatile organic compounds (SVOCs) into house dust: from multilayer to monolayer. Build. Environ. 233, 110084. https://doi.org/10.1016/j.buildenv.2023.110084.

Chen, F., Lin, Y., Cai, M., Zhang, J., Zhang, Y., Kuang, W., Liu, L., Huang, P., Ke, H., 2018a. Occurrence and risk assessment of PAHs in surface sediments from Western arctic and subarctic oceans. Int. J. Environ. Res. Publ. Health 15, 734. https://doi.org/10.3390/ijerph15040734.

Chen, Y., Sun, C., Zhang, J., Zhang, F., 2018b. Assessing 16 polycyclic aromatic Hydrocarbons(PAHs) in river basin water and SedimentRegarding spatial-temporal Distribution,Partitioning, and ecological risks. Pol. J. Environ. Stud. 27, 579–589. https://doi.org/10.15244/pjoes/75827.

Chu, W.-L., Dang, N.-L., Kok, Y.-Y., Ivan Yap, K.-S., Phang, S.-M., Convey, P., 2019. Heavy metal pollution in Antarctica and its potential impacts on algae. Polar Sci. 20, 75–83. https://doi.org/10.1016/j.polar.2018.10.004.

Cordero, R.R., Sepúlveda, E., Feron, S., Damiani, A., Fernandoy, F., Neshyba, S., Rowe, P. M., Asencio, V., Carrasco, J., Alfonso, J.A., Llanillo, P., Wachter, P., Seckmeyer, G., Stepanova, M., Carrera, J.M., Jorquera, J., Wang, C., Malhotra, A., Dana, J., Khan, A. L., Casassa, G., 2022. Black carbon footprint of human presence in Antarctica. Nat. Commun. 13, 984. https://doi.org/10.1038/s41467-022-28560-w.

Cox, S.C., Smith Lyttle, B., Elkind, S., Smith Siddoway, C., Morin, P., Capponi, G., Abu-Alam, T., Ballinger, M., Bamber, L., Kitchener, B., Lelli, L., Mawson, J., Millikin, A., Dal Seno, N., Whitburn, L., White, T., Burton-Johnson, A., Crispini, L., Elliot, D., Elvevold, S., Goodge, J., Halpin, J., Jacobs, J., Martin, A.P., Mikhalsky, E., Morgan, F., Scadden, P., Smellie, J., Wilson, G., 2023. A continent-wide detailed geological map dataset of Antarctica. Sci. Data 10, 250. https://doi.org/10.1038/s41597-023-02152-9.

Davies, B., Bendle, J., Glasser, N., García, J.-L., Kaplan, M., 2023. Editorial: glaciation and climate change in the andean Cordillera. Front. Earth Sci. 11, 1129795. https://doi.org/10.3389/feart.2023.1129795.

Davis, E., Walker, T.R., Adams, M., Willis, R., Norris, G.A., Henry, R.C., 2019. Source apportionment of polycyclic aromatic hydrocarbons (PAHs) in small craft harbor (SCH) surficial sediments in Nova Scotia. Canada. Sci. Total Environ. 691, 528–537. https://doi.org/10.1016/j.scitotenv.2019.07.114.

Deka, J.P., Dash, S., Sandil, S., Chaminda, T., Mahlknecht, J., Kumar, M., 2024. Long-range transport of polycyclic aromatic hydrocarbons and metals in high altitude lacustrine environments of the eastern himalayas: speciation, and source apportionment perspectives. ACS ES&T Water 4, 3400–3411. https://doi.org/10.1021/acsestwater.4c00255.

Dickhut, R.M., Cincinelli, A., Cochran, M., Ducklow, H.W., 2005. Atmospheric concentrations and air–water flux of organochlorine pesticides along the Western antarctic peninsula. Environ. Sci. Technol. 39, 465–470. https://doi.org/10.1021/es048648p.

Draxler, R.R., Hess, G.D., n.d. NOAA Technical Memorandum ERL ARL-224.

Drotikova, T., Ali, A.M., Halse, A.K., Reinardy, H.C., Kallenborn, R., 2020. Polycyclic aromatic hydrocarbons (PAHs) and oxy- and nitro-PAHs in ambient air of the arctic town longyearbyen, Svalbard. Atmos. Chem. Phys. 20, 9997–10014. https://doi.org/10.5194/acp-20-9997-2020.

Fang, X., Saito, T., Park, S., Li, S., Yokouchi, Y., Prinn, R.G., 2018. Performance of back-trajectory statistical methods and inverse modeling method in locating emission sources. ACS Earth Space Chem. 2, 843–851. https://doi.org/10.1021/acsearthspacechem.8b00062.

Fernandoy, F., Tetzner, D., Meyer, H., Gacitúa, G., Hoffmann, K., Falk, U., Lambert, F., MacDonell, S., 2018. New insights into the use of stable water isotopes at the northern antarctic peninsula as a tool for regional climate studies. Cryosphere 12, 1069–1090. https://doi.org/10.5194/tc-12-1069-2018.

Friedman, C.L., Selin, N.E., 2012. Long-range atmospheric transport of polycyclic aromatic hydrocarbons: a global 3-D model analysis including evaluation of arctic sources. Environ. Sci. Technol. 46, 9501–9510. https://doi.org/10.1021/es301904d.

Gambaro, A., Manodori, L., Zangrando, R., Cincinelli, A., Capodaglio, G., Cescon, P., 2005. Atmospheric PCB concentrations at Terra nova Bay, Antarctica. Environ. Sci. Technol. 39, 9406–9411. https://doi.org/10.1021/es0510921.

Gebru, T.B., Zhang, Q., Dong, C., Hao, Y., Li, C., Yang, R., Li, Y., Jiang, G., 2024. The long-term spatial and temporal distributions of polychlorinated naphthalene air concentrations in fildes peninsula, west Antarctica. J. Hazard Mater. 463, 132824. https://doi.org/10.1016/j.jhazmat.2023.132824.

González, J., Romero-Aguilar, L., Matus-Ortega, G., Pablo Pardo, J., Flores-Alanis, A., Segal-Kischinevzky, C., 2020. Levaduras adaptadas al frío: el tesoro biotecnológico de la Antártica. Tip. Rev. Espec. Ciencias Químico-Biol. 23. https://doi.org/10.22201/fesz.23958723e.2020.0.267.

Han, B., Wang, G., Liu, A., Zheng, Y., Zheng, L., Ding, R., 2023. Characteristics and source analysis of polycyclic aromatic hydrocarbons in organisms and manure near ardley island, Antarctica. Mar. Pollut. Bull. 188, 114577. https://doi.org/10.1016/j.marpolbul.2023.114577.

Hayakawa, K., Tang, N., Nagato, E.G., Toriba, A., Aoki, K., 2019. Identification of long-range transported polycyclic aromatic hydrocarbons in snow at Mt. Tateyama, Japan. Aerosol Air Qual. Res. 19, 1252–1258. https://doi.org/10.4209/aaqr.2018.05.0153.

Hegg, D.A., Warren, S.G., Grenfell, T.C., Sarah, J Doherty, Clarke, A.D., 2010. Sources of light-absorbing aerosol in arctic snow and their seasonal variation. Atmos. Chem. Phys. 10, 10923–10938. https://doi.org/10.5194/acp-10-10923-2010.

Hoffmann-Abdi, K., Meyer, H., Fernandoy, F., Freitag, J., Shaw, F.M., Werner, M., Thomas, E.R., McConnell, J.R., Schneider, C., 2023. Deciphering stable water isotope records of firn cores from a strongly maritime, high-accumulation site on the antarctic peninsula. J. Glaciol. 69, 2027–2045. https://doi.org/10.1017/jog.2023.79.

Iriarte, J., Dachs, J., Casas, G., Martínez-Varela, A., Berrojalbiz, N., Vila-Costa, M., 2023. Snow-dependent biogeochemical cycling of polycyclic aromatic hydrocarbons at coastal Antarctica. Environ. Sci. Technol. 57, 1625–1636. https://doi.org/10.1021/acs.est.2c05583.

Kallenborn, R., 2006. Persistent organic pollutants (POPs) as environmental risk factors in remote high-altitude ecosystems. Ecotoxicol. Environ. Saf. 63, 100–107. https://doi.org/10.1016/j.ecoenv.2005.02.016.

Kallenborn, R., Oehme, M., Wynn-Williams, D.D., Schlabach, M., Harris, J., 1998. Ambient air levels and atmospheric long-range transport of persistent organochlorines to signy island, Antarctica. Sci. Total Environ. 220, 167–180. https://doi.org/10.1016/S0048-9697(98)00257-5.

Katsoyiannis, A., Terzi, E., Cai, Q.-Y., 2007. On the use of PAH molecular diagnostic ratios in sewage sludge for the understanding of the PAH sources. Is this use appropriate? Chemosphere 69, 1337–1339. https://doi.org/10.1016/j.chemosphere.2007.05.084.

Keyte, I.J., Harrison, R.M., Lammel, G., 2013a. Chemical reactivity and long-range transport potential of polycyclic aromatic hydrocarbons – a review. Chem. Soc. Rev. 42, 9333. https://doi.org/10.1039/c3cs60147a.

Keyte, I.J., Harrison, R.M., Lammel, G., 2013b. Chemical reactivity and long-range transport potential of polycyclic aromatic hydrocarbons – a review. Chem. Soc. Rev. 42, 9333. https://doi.org/10.1039/c3cs60147a.

Kozhevnikov, A.Yu, Falev, D.I., Sypalov, S.A., Kozhevnikova, I.S., Kosyakov, D.S., 2021. Polycyclic aromatic hydrocarbons in the snow cover of the northern city agglomeration. Sci. Rep. 11, 19074. https://doi.org/10.1038/s41598-021-98386-x.

Kubo, T., Bai, W., Nagae, M., Takao, Y., 2020. Seasonal fluctuation of polycyclic aromatic hydrocarbons and aerosol genotoxicity in long-range transported air mass observed at the Western end of Japan. Int. J. Environ. Res. Publ. Health 17, 1210. https://doi.org/10.3390/ijerph17041210.

Kukučka, P., Lammel, G., Dvorská, A., Klánová, J., Möller, A., Fries, E., 2010. Contamination of antarctic snow by polycyclic aromatic hydrocarbons dominated by combustion sources in the polar region. Environ. Chem. 7, 504. https://doi.org/10.1071/EN10066.

Lammel, G., 2015. Long-range atmospheric transport of polycyclic aromatic hydrocarbons is worldwide problem - results from measurements at remote sites and modelling. Acta Chim. Slov. 729–735. https://doi.org/10.17344/acsi.2015.1387.

Liu, X., Dong, Z., Baccolo, G., Gao, W., Li, Q., Wei, T., Qin, X., 2023. Distribution, composition and risk assessment of PAHs and PCBs in cryospheric watersheds of the eastern Tibetan Plateau. Sci. Total Environ. 890, 164234. https://doi.org/10.1016/j.scitotenv.2023.164234.

Ma, Y., Xie, Z., Yang, H., Möller, A., Halsall, C., Cai, M., Sturm, R., Ebinghaus, R., 2013. Deposition of polycyclic aromatic hydrocarbons in the north Pacific and the arctic. J. Geophys. Res. Atmospheres 118, 5822–5829. https://doi.org/10.1002/jgrd.50473.

Miura, K., Shimada, K., Sugiyama, T., Sato, K., Takami, A., Chan, C.K., Kim, I.S., Kim, Y. P., Lin, N.-H., Hatakeyama, S., 2019. Seasonal and annual changes in PAH concentrations in a remote site in the Pacific Ocean. Sci. Rep. 9, 12591. https://doi.org/10.1038/s41598-019-47409-9.

Müller, A., Österlund, H., Marsalek, J., Viklander, M., 2022. Exploiting urban roadside snowbanks as passive samplers of organic micropollutants and metals generated by traffic. Environ. Pollut. 308, 119723. https://doi.org/10.1016/j.envpol.2022.119723.

Na, G., Liu, C., Wang, Z., Ge, L., Ma, X., Yao, Z., 2011. Distribution and characteristic of PAHs in snow of fildes peninsula. J. Environ. Sci. 23, 1445–1451. https://doi.org/10.1016/S1001-0742(10)60605-5.

Neira, C., Cossaboon, J., Mendoza, G., Hoh, E., Levin, L.A., 2017. Occurrence and distribution of polycyclic aromatic hydrocarbons in surface sediments of San Diego Bay marinas. Mar. Pollut. Bull. 114, 466–479. https://doi.org/10.1016/j.marpolbul.2016.10.009.

Pawlak, F., Koziol, K., Polkowska, Z., 2021. Chemical hazard in glacial melt? The glacial system as a secondary source of POPs (in the northern hemisphere). A systematic review. Sci. Total Environ. 778, 145244. https://doi.org/10.1016/j.scitotenv.2021.145244.

Pei, L., Yan, Z., Chen, D., Miao, S., 2020. Climate variability or anthropogenic emissions: which caused beijing haze? Environ. Res. Lett. 15, 034004. https://doi.org/10.1088/1748-9326/ab6f11.

Puasa, N.A., Zulkharnain, A., Verasoundarapandian, G., Wong, C.-Y., Zahri, K.N.M., Merican, F., Shaharuddin, N.A., Gomez-Fuentes, C., Ahmad, S.A., 2021. Effects of diesel, heavy metals and plastics pollution on penguins in Antarctica: a review. Animals 11, 2505. https://doi.org/10.3390/ani11092505.

Qin, Y., Wu, T., Zhao, L., Wu, X., Li, R., Xie, C., Pang, Q., Hu, G., Qiao, Y., Zhao, G., Liu, G., Zhu, X., Hao, J., 2017. Numerical modeling of the active layer thickness and permafrost thermal state across qinghai-tibetan Plateau. J. Geophys. Res. Atmospheres 122. https://doi.org/10.1002/2017JD026858.

Salat, A.P.J., Eickmeyer, D.C., Kimpe, L.E., Hall, R.I., Wolfe, B.B., Mundy, L.J., Trudeau, V.L., Blais, J.M., 2021. Integrated analysis of petroleum biomarkers and polycyclic aromatic compounds in Lake sediment cores from an oil sands region. Environ. Pollut. 270, 116060. https://doi.org/10.1016/j.envpol.2020.116060.

Shunthirasingham, C., Barra, R., Mendoza, G., Montory, M., Oyiliagu, C.E., Lei, Y.D., Wania, F., 2011. Spatial variability of atmospheric semivolatile organic compounds in Chile. Atmos. Environ. 45, 303–309. https://doi.org/10.1016/j.atmosenv.2010.10.027.

Steenhuisen, F., Van Den Heuvel-Greve, M., 2021. Exposure radius of a local coal mine in an arctic coastal system; correlation between PAHs and Mercury as a marker for a local mercury source. Environ. Monit. Assess. 193, 499. https://doi.org/10.1007/s10661-021-09287-5.

Stein, A.F., Draxler, R.R., Rolph, G.D., Stunder, B.J.B., Cohen, M.D., Ngan, F., 2015. NOAA's HYSPLIT atmospheric transport and dispersion modeling system. Bull. Am. Meteorol. Soc. 96, 2059–2077. https://doi.org/10.1175/BAMS-D-14-00110.1.

Strugnell, J.M., McGregor, H.V., Wilson, N.G., Meredith, K.T., Chown, S.L., Lau, S.C.Y., Robinson, S.A., Saunders, K.M., 2022. Emerging biological archives can reveal ecological and climatic change in Antarctica. Glob. Change Biol. 28, 6483–6508. https://doi.org/10.1111/gcb.16356.

Szopińska, M., Szumińska, D., Bialik, R.J., Dymerski, T., Rosenberg, E., Polkowska, Ż., 2019. Determination of polycyclic aromatic hydrocarbons (PAHs) and other organic pollutants in freshwaters on the western shore of admiralty Bay (king george island, maritime Antarctica). Environ. Sci. Pollut. Res. 26, 18143–18161. https://doi.org/10.1007/s11356-019-05045-w.

Thompson, N., Adjei, J.K., Bentum, J.K., Essumang, D.K., Duodu, G.O., Hadzi, G., Adjei, G.A., 2022. Vehicular influence on atmospheric concentrations and source apportionment of polycyclic aromatic hydrocarbons in some major cities in three regions of Ghana using epiphytic lichens. Toxicol. Rep. 9, 1691–1699. https://doi.org/10.1016/j.toxrep.2022.08.002.

Tin, T., Fleming, Z.L., Hughes, K.A., Ainley, D.G., Convey, P., Moreno, C.A., Pfeiffer, S., Scott, J., Snape, I., 2009. Impacts of local human activities on the antarctic environment. Antarct. Sci. 21, 3–33. https://doi.org/10.1017/S0954102009001722.

Tobiszewski, M., Namieśnik, J., 2012. PAH diagnostic ratios for the identification of pollution emission sources. Environ. Pollut. 162, 110–119. https://doi.org/10.1016/j.envpol.2011.10.025.

Van Overmeiren, P., Demeestere, K., De Wispelaere, P., Gili, S., Mangold, A., De Causmaecker, K., Mattielli, N., Delcloo, A., Langenhove, H.V., Walgraeve, C., 2024. Four years of active sampling and measurement of atmospheric polycyclic aromatic hydrocarbons and oxygenated polycyclic aromatic hydrocarbons in dronning maud land, east Antarctica. Environ. Sci. Technol. 58, 1577–1588. https://doi.org/10.1021/acs.est.3c06425.

Vecchiato, M., Barbante, C., Barbaro, E., Burgay, F., Cairns, W.Rl, Callegaro, A., Cappelletti, D., Dallo, F., D'Amico, M., Feltracco, M., Gallet, J.-C., Gambaro, A., Larose, C., Maffezzoli, N., Mazzola, M., Sartorato, I., Scoto, F., Turetta, C., Vardè, M., Xie, Z., Spolaor, A., 2024. The seasonal change of PAHs in Svalbard surface snow. Environ. Pollut. 340, 122864. https://doi.org/10.1016/j.envpol.2023.122864.

Vecchiato, M., Barbaro, E., Spolaor, A., Burgay, F., Barbante, C., Piazza, R., Gambaro, A., 2018. Fragrances and PAHs in snow and seawater of Ny-Ålesund (svalbard): local and long-range contamination. Environ. Pollut. 242, 1740–1747. https://doi.org/10.1016/j.envpol.2018.07.095.

Vilanova, R.M., Fernández, P., Martinez, C., Grimalt, J.O., 2001. Polycyclic aromatic hydrocarbons in remote mountain lake waters. Water Res. 35, 3916–3926. https://doi.org/10.1016/S0043-1354(01)00113-0.

Wang, S.-Q., Hu, Y.-J., Yuan, Y.-F., Hu, Z.-C., Wu, C.-C., Bao, L.-J., Zeng, E.Y., 2023. Size-resolved gas-particle partitioning characteristics of typical semi-volatile organic compounds in urban atmosphere. Environ. Pollut. 320, 121101. https://doi.org/10.1016/j.envpol.2023.121101.

Wang, X., Gong, P., Sheng, J., Joswiak, D.R., Yao, T., 2015. Long-range atmospheric transport of particulate polycyclic aromatic hydrocarbons and the incursion of aerosols to the southeast Tibetan Plateau. Atmos. Environ. 115, 124–131. https://doi.org/10.1016/j.atmosenv.2015.04.050.

Wania, F., Mackay, D., 1995. A global distribution model for persistent organic chemicals. Sci. Total Environ. 160–161, 211–232. https://doi.org/10.1016/0048-9697(95)04358-8.

Wei, L., Lv, J., Zuo, P., Li, Y., Yang, R., Zhang, Q., Jiang, G., 2024. The occurrence and sources of PAHs, oxygenated PAHs (OPAHs), and nitrated PAHs (NPAHs) in soil and vegetation from the antarctic, arctic, and Tibetan Plateau. Sci. Total Environ. 912, 169394. https://doi.org/10.1016/j.scitotenv.2023.169394.

Wilson, J., Pöschl, U., Shiraiwa, M., Berkemeier, T., 2021. Non-equilibrium interplay between gas–particle partitioning and multiphase chemical reactions of semi-volatile compounds: mechanistic insights and practical implications for atmospheric modeling of polycyclic aromatic hydrocarbons. Atmos. Chem. Phys. 21, 6175–6198. https://doi.org/10.5194/acp-21-6175-2021.

Wu, Q., Cao, S., Chen, Z., Wei, X., Ma, G., Yu, H., 2022. Predictive models of gas/particulate partition coefficients (KP) for polycyclic aromatic hydrocarbons and their oxygen/nitrogen derivatives. Molecules 27, 7608. https://doi.org/10.3390/molecules27217608.

Wu, X., Wang, J., Yuan, Z., Wang, S., 2023a. Polycyclic aromatic compounds (PACs) in tree barks and tree cores of a national large-scale coal-fired power base of China: sources, atmospheric toxicities, and pollution histories. Sci. Total Environ. 879, 163045. https://doi.org/10.1016/j.scitotenv.2023.163045.

Wu, Z., Lin, T., Sun, H., Li, R., Liu, X., Guo, Z., Ma, X., Yao, Z., 2023b. Polycyclic aromatic hydrocarbons in fildes peninsula, maritime Antarctica: effects of human disturbance. Environ. Pollut. 318, 120768. https://doi.org/10.1016/j.envpol.2022.120768.

Xie, Z., Kallenborn, R., 2023. Legacy and emerging per- and poly-fluoroalkyl substances in polar regions. Curr. Opin. Green Sustainable Chem. 42, 100840. https://doi.org/10.1016/j.cogsc.2023.100840.

Xie, Z., Zhang, P., Wu, Z., Zhang, S., Wei, L., Mi, L., Kuester, A., Gandrass, J., Ebinghaus, R., Yang, R., Wang, Z., Mi, W., 2022. Legacy and emerging organic contaminants in the polar regions. Sci. Total Environ. 835, 155376. https://doi.org/10.1016/j.scitotenv.2022.155376.

Yu, Y., Katsoyiannis, A., Bohlin-Nizzetto, P., Brorström-Lundén, E., Ma, J., Zhao, Y., Wu, Z., Tych, W., Mindham, D., Sverko, E., Barresi, E., Dryfhout-Clark, H., Fellin, P., Hung, H., 2019. Polycyclic aromatic hydrocarbons not declining in arctic air despite global emission reduction. Environ. Sci. Technol. 53, 2375–2382. https://doi.org/10.1021/acs.est.8b05353.

Yunker, M.B., Macdonald, R.W., Vingarzan, R., Mitchell, R.H., Goyette, D., Sylvestre, S., 2002. PAHs in the fraser river basin: a critical appraisal of PAH ratios as indicators of PAH source and composition. Org. Geochem. 33, 489–515. https://doi.org/10.1016/S0146-6380(02)00002-5.

Zhang, L., Cheng, I., Muir, D., Charland, J.-P., 2015. Scavenging ratios of polycyclic aromatic compounds in rain and snow in the athabasca oil sands region. Atmos. Chem. Phys. 15, 1421–1434. https://doi.org/10.5194/acp-15-1421-2015.